Viscoelastic Properties and Shock Response of Coarse-Grained Models of Multiblock versus Diblock Copolymers: Insights into Dissipative Properties of Polyurea

ARTICLE *in* MACROMOLECULES · APRIL 2012

Impact Factor: 5.8 · DOI: 10.1021/ma3001934

3 AUTHORS, INCLUDING:

Bedri Arman

11 PUBLICATIONS **186** CITATIONS

SEE PROFILE

Gaurav Arya

University of California, San Diego

68 PUBLICATIONS **1,367** CITATIONS

SEE PROFILE

Macromolecules

Article

pubs.acs.org/Macromolecules

Viscoelastic Properties and Shock Response of Coarse-Grained Models of Multiblock versus Diblock Copolymers: Insights into Dissipative Properties of Polyurea

Bedri Arman, A. Srinivas Reddy, and Gaurav Arya*

Department of NanoEngineering, University of California, San Diego, 9500 Gilman Drive, Mail Code 0448, La Jolla, California 92093, United States

Supporting Information

ABSTRACT: We compare and contrast the microstructure, viscoelastic properties, and shock response of coarse-grained models of multiblock copolymer and diblock copolymers using molecular dynamics simulations. This study is motivated by the excellent dissipative and shock-mitigating properties of polyurea, speculated to arise from its multiblock chain architecture. Our microstructural analyses reveal that the multiblock copolymer microphase-separates into small, interconnected, rod-shaped, hard domains surrounded by a soft matrix, whereas the diblock copolymer forms larger, unconnected, hard domains. Our viscoelastic analyses indicate that compared with the diblock copolymer, the multiblock copolymer is not only more elastic but also more dissipative, as signified by its larger storage and loss modulus at low to intermediate frequencies. Our shock simulations and slip analyses reveal that shock waves propagate slower in the multiblock copolymer in comparison with the diblock copolymer, most likely due to the more deformable hard domains in the former system. These results suggest that the multiblock architecture of polyurea might impart polyurea with smaller, more deformable, and interconnected hard domains that lead to improved energy dissipation and lower shock speeds.

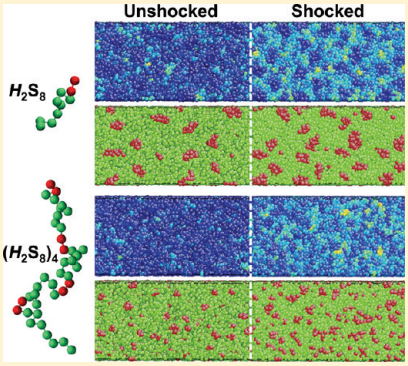

1. INTRODUCTION

Polyurea is a polymer formed by the reaction of a difunctional amine ($H_2N-R-NH_2$) and a difunctional isocyanate (OCN−R′−NCO). In general, R is a linear hydrocarbon chain and R′ an aromatic moiety, which make polyurea a multiblock polymer with alternating soft (R) and hard (R′) segments along its backbone (Figure 1a). Hydrogen bonding across distinct urea linkages (−HN−CO−NH−) along with possible Π-stacking interactions between aromatic rings cause the rigid segments to self-assemble and form high-T_g (glass-transition temperature), rod-shaped hard domains dispersed within a low-T_g soft matrix composed of the linear hydrocarbon chains.[1] At room temperature, the soft domains are above their T_g and impart polyurea its elastomeric properties, whereas the hard domains are below their T_g and impart polyurea its mechanical toughness and compressive stiffness, allowing polyurea to be used in a wide range of coating applications.[2,3] More recently, polyurea has been found to possess good dissipative properties and thus has been used as a shock-resistant material, especially to prevent the traumatic brain injury resulting from impacts and blasts.[4−6]

Whereas some ideas along the lines of a rubbery-to-glassy phase transformation within polyurea,[4] resonance of hard domains at high frequencies,[7] and breakage of hydrogen bonds across urea linkage[8] accompanying an impact have been proposed, a clear understanding of the mechanisms responsible for the superior energy dissipation properties of polyurea is still lacking. The dissipative nature of polyurea could arise from its "multiblock" architecture—repeating units of hard and soft segments. Interestingly, such a chain structure allows for the microphase-separated hard domains to remain covalently linked to each other via the soft segments, as the hard segments in one chain could conceivably participate in more than one hard domain. Such connectivity between the hard domains would not be achievable in a "diblock" version of polyurea possessing only a single hard and soft segment. In addition, because of the larger number of restrictions imposed on the multiblock copolymer chains compared with its diblock equivalent, the hard domains in multiblock polyurea are expected to be smaller and less stable than those of a diblock polyurea. These restrictions include entropy loss and bending penalty on the soft segments to permit the intervening or flanking hard segments to participate in a hard domain. How the multiblock chain architecture of polyurea, or any polymer for that matter, might enhance its energy dissipation and shock-mitigation properties clearly calls for a more detailed examination.

Here we take the first step toward addressing this question by carrying out a detailed comparison of the microstructure, viscoelastic properties, and shock response of a polyurea-like multiblock copolymer, a diblock copolymer, and two homopolymers. Our approach is computational, involving the use of idealized coarse-grained models to treat the four

Received: January 25, 2012
Revised: March 19, 2012
Published: March 28, 2012

polymers and the use of molecular dynamics (MD) simulations to compute their bulk properties. Because the study is motivated by polyurea, the composition of the hard and soft segments in our multiblock copolymer and their segregation strength are chosen to be roughly compatible with that of polyurea. However, no attempts have been made to rigorously map our multiblock copolymer chains onto polyurea to keep the model sufficiently generic and applicable to other multiblock copolymer systems that microphase-separate into well-segregated hard and soft domains. The diblock copolymer used for comparison is taken to be a shortened version of the multiblock copolymer, possessing a single hard and soft segment, and the homopolymers are taken to be of similar molecular weight as the two block copolymers but possess only the soft segments. Not only would the results from this study be relevant to the design of next-generation elastomeric materials for blast mitigation but also they would be of general interest to the polymers community, as this study represents to the best of our knowledge the first detailed computational investigation of the viscoelastic and shock response of block copolymers.

The rest of this Article is organized as follows. In Section 2, we describe coarse-grained modeling of the four polymer systems and the computation of their microstructure, viscoelastic properties, and shock response via MD simulations. In Section 3, we compare the polymeric systems in terms of chain configurations, monomer distributions, domain morphology, dynamic shear modulus, loss and storage modulus, shock velocities, and slip profiles. In Section 4, we discuss how these results provide useful insight into the superior dissipative properties of polyurea and suggest possible future extensions.

2. METHODS

Coarse-Grained Modeling of Polymers. We examine four polymeric systems in this study: a polyurea-like multiblock copolymer composed of hard and soft segments, a diblock version of the multiblock copolymer, and two homopolymers of soft segments with the same chain lengths as the multiblock and diblock copolymers. We employ the coarse-grained, bead-chain model of Kremer and Grest[9] to treat the four types of polymer chains. In this model, segments of the polymer are treated as coarse-grained beads of size σ and mass m. Two different types of beads denoted by H and S are employed to treat the hard and soft segments in the block copolymer chains, respectively. The number of beads of each type and their size are assigned according to the polyurea chain shown in Figure 1a, which is synthesized from the reaction of a diphenylmethane diisocyanate (hard segment) and a poly(tetramethylene oxide)-diaminobenzoate (soft segment) and is extensively used for blast mitigation.[10−12] Specifically, two H beads with σ = 11.2 Å and m = 150.6 amu are used to represent the hard segment of polyurea, and eight S beads of the same size as the H beads are used to represent the soft segment. The *diblock* version of polyurea thus comprises of a total of 10 beads and is denoted by H_2S_8 (Figure 1b). The *multiblock* chain is composed of four repeating units of the diblock copolymer (i.e., total of 40 beads) and is denoted by $(H_2S_8)_4$ (Figure 1c). Note that the degree of polymerization of experimental polyurea chains is much larger, but computational limitations preclude us from simulating chains longer than 40 beads. The *homopolymer* versions of the diblock and multiblock copolymers are composed of 10 and 40 soft beads and are denoted by S_{10} and S_{40}, respectively.

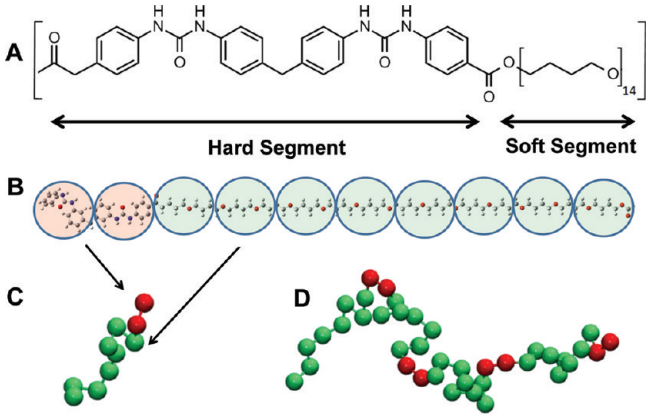

Figure 1. (a) Chemical structure of polyurea and (b) its mapping onto a coarse-grained bead−spring model. The hard segment is represented by two H beads (red), and the soft segment is represented by eight S beads (green). This mapping yields the (c) H_2S_8 and (d) $(H_2S_8)_4$ models of the diblock and multiblock copolymer.

The adjacent beads in all four polymer chains—$(H_2S_8)_4$, H_2S_8, S_{40}, and S_{10}—are connected via a strong finitely extensible nonlinear elastic (FENE) potential

$$U_{\mathrm{FENE}} = -\frac{k}{2}R_0^2 \ln[1 - (r/R_0)^2] \quad (1)$$

where r is the distance between bonded beads, $R_0 = 1.5\sigma$ is the maximum possible length of the spring, and $k = 30\varepsilon/\sigma^2$ is the spring constant. The parameter ε sets the energy scale (see below).

All $S-S$ and $H-S$ nonbonded interactions are treated using a short-range purely repulsive potential, also known as the Weeks−Chandler−Anderson (WCA) potential[13]

$$U_{\mathrm{rep}} = \begin{cases} 4\varepsilon[(\sigma/r)^{12} - (\sigma/r)^6 + 1/4] & r < 2^{1/6}\sigma \\ 0 & r \geq 2^{1/6}\sigma \end{cases} \quad (2)$$

All $H-H$ nonbonded interactions are treated using a short-range potential that includes both repulsive and attractive components[14,15]

$$U_{\mathrm{att}} = \begin{cases} 4\varepsilon[(\sigma/r)^{12} - (\sigma/r)^6 + 1/4] - \Phi & r < 2^{1/6}\sigma \\ \frac{1}{2}\Phi[\cos(\alpha r^2 + \beta) - 1] & 2^{1/6}\sigma \leq r < 1.5\sigma \\ 0 & r \geq 1.5\sigma \end{cases} \quad (3)$$

In U_{att}, the constants α = 3.17307 and β = −0.85623 are chosen so that the potential is continuous and approaches smoothly to zero at the cutoff distance and Φ represents the attractive well depth of this potential and is responsible for promoting microphase separation in our two block copolymers.

The parameter Φ represents the "effective" attraction between the $H-H$ segments and is given by $E_{HH} + E_{SS} - 2E_{HS}$, where E_{ij} are the "actual" attraction energies for the three pairs of interactions. According to previous studies,[16,17] we choose $\Phi = 2.5\varepsilon$ and $\varepsilon = k_BT$, which are known to yield strongly segregated microphases. Moreover, rough calculations show that the chosen value of Φ yields a dimensionless Flory−Huggins parameter χ_{HS} close to a previously reported value for polyurea. Specifically, χ_{HS} for our system can be computed

dx.doi.org/10.1021/ma3001934 | Macromolecules 2012, 45, 3247−3255

using the standard relation $\chi_{HS} = z\Delta w/k_BT$, where z is the average coordination number of the polymer segments (beads) and Δw is an energy parameter that is a function of the individual pairwise contact energies of the hard and soft beads: $\Delta w = w_{HS} - 1/2(w_{HH} + w_{SS})$.[18] Using $z \approx 5$, as estimated from Cahoon's chart,[19] $w_{HS} = w_{SS} = 0$, and $w_{HH}/k_BT = -\Phi$, we obtain $\chi_{HS} \approx 6.25$, which is close to the value of 5.42 reported by Grujicic et al.[20]

For convenience, we report our results in reduced units of bead mass m, size σ, and energy ε. These quantities in reduced units, identified by asterisks, can be converted to real units, without asterisks, as follows: time $t^* = t(\varepsilon/m\sigma^2)^{1/2}$, frequency $\omega^* = \omega(m\sigma^2/\varepsilon)^{1/2}$, length $l^* = l/\sigma$, temperature $T^* = k_BT/\varepsilon$, energy $E^* = E/\varepsilon$, pressure $P^* = P\sigma^3/\varepsilon$, viscosity $\eta^* = \eta\sigma^2/(m\varepsilon)^{1/2}$, speed $u^* = u(m/\varepsilon)^{1/2}$, moduli $G^* = G\sigma^3/\varepsilon$, and number density $\rho^* = \rho\sigma^3$. From this point onward, we report only reduced values but omit the asterisks for convenience, unless otherwise noted.

Calculation of Polymer Properties. The microstructure and viscoelastic properties of the four polymer systems previously introduced are computed using equilibrium MD simulations performed in the canonical (NVT) ensemble. In our simulations, we set the temperature T to a value of 1 using a Nosé–Hoover thermostat.[21] A standard velocity-Verlet algorithm is used to integrate the equations of motion with a time step of $\Delta t = 0.012$ similar to previous studies.[22,23] The initial configurations are generated by placing linear chains in a large simulation box implementing periodic boundary conditions (PBCs). The simulation box is then gradually compressed until the bead density ρ reaches a value of 0.85. At the chosen density and temperature, the soft segments are above their T_g and exist in a melt state,[9] the hard segments are below their T_g and display a solid state,[17] and the entire system is below the order–disorder transition temperature.[17] During this compression step, only the repulsive pair interactions (eq 2) are implemented. In the two block copolymer systems, the attractive interactions are turned on after the relaxation of the chains at the same density. We utilize system sizes composed of $n = 20\,000$ and $80\,000$ total beads for determining the viscoelastic properties and microstructure, respectively. The simulations are run for 2×10^7 and 4×10^7 time steps for the homopolymers and block copolymers, respectively. Assuming ε to be on the order of k_BT at room temperature, the time step is ~0.1 ps and the simulations span ~2–4 μs of real time.

The time-dependent shear modulus $G(t)$ is computed from the stress autocorrelation function (SACF)

$$G(t) = \frac{V}{k_BT}\langle \sigma_{\alpha\beta}(t)\sigma_{\alpha\beta}(0)\rangle \tag{4}$$

and the Newtonian shear viscosity η is computed using the Green–Kubo formulation

$$\eta = \int_0^\infty G(t)\, dt \tag{5}$$

where V is the system volume, T is the temperature, k_B is the Boltzmann constant, and $\langle\cdots\rangle$ denotes ensemble average. The stress $\sigma_{\alpha\beta}$ is calculated via the virial theorem

$$\sigma_{\alpha\beta} = \frac{1}{V}\left[\sum_{i=1}^{n} m_i v_{i\alpha} v_{i\beta} + \sum_{i=1}^{n-1}\sum_{j=i+1}^{n} r_{ij\alpha} F_{ij\beta}\right] \tag{6}$$

Here m_i, $v_{i\alpha}$, and $v_{i\beta}$ are the mass and α- and β-component velocities of bead i, respectively; and $r_{ij\alpha}$ and $F_{ij\beta}$ are the α-component separation distance and β-component force acting between beads i and j, respectively. The first term specifies the kinetic energy contribution, and the second term specifies the bonded and nonbonded energy contributions. Note that the three off-diagonal elements of the stress tensor σ_{xy}, σ_{xz}, and σ_{yz} are equivalent, as expected for an isotropic system. We therefore use the average of the three stresses to obtain smoother estimates of the SACF. Furthermore, the stresses are computed each time step to obtain accurate results, as done in previous studies.[24]

The storage modulus $G'(\omega)$ and the loss modulus $G''(\omega)$ are computed by converting $G(t)$ into its frequency (ω)-dependent complex form $G^*(\omega)$

$$G^*(\omega) = i\omega \int_0^\infty e^{-i\omega t} G_{xy}(t)\, dt \tag{7}$$

where $G'(\omega)$ and $G''(\omega)$ represent the real and complex portions of $G^*(\omega)$, respectively

$$G'(\omega) = \omega \int_0^\infty G_{xy}(t)\sin(\omega t)\, dt \tag{8}$$

$$G''(\omega) = \omega \int_0^\infty G_{xy}(t)\cos(\omega t)\, dt \tag{9}$$

In shock simulations, a sufficiently long simulation box along the direction of wave propagation is required. To this end, the simulation box used for computing viscoelastic properties is replicated ×12 along the chosen direction for shock propagation (z-axis), yielding a box of sides 28.7 × 28.7 × 338 containing 240 000 beads. The PBCs are implemented only along the two directions orthogonal to the shock direction and equilibrated to a pressure $P \approx 0$ in an NPT ensemble, which is nominal for shock simulations. The resulting configuration is then used as the starting point for the shock simulations. The shock runs are performed by adopting the projectile-wall geometry and a microcanonical (NVE) ensemble to mimic adiabatic conditions.[25−27] In this approach, the desired "particle" velocity u_p pointing in the $+z$ direction is added to the thermal velocity of each polymer bead. The simulation box dimensions are fixed along the x and y directions such that a 1D strain loading mimicking the experiments is generated. Upon the impact of polymer beads with the wall located at the $+z$ end of the simulation box, a shock wave is generated that travels away from the wall in the direction opposite to u_p. The energetic interaction between the wall particles and the polymer beads are treated using a 12–6 Lennard-Jones potential.[27]

To characterize atomic-level deformations of the polymer in the shocked and unshocked regions, we compute the slip vector s_i, which is defined as the maximum relative displacement[27,28] of bead i with respect to its j neighbors

$$\mathbf{s}_i \equiv \max(\mathbf{x}_{ij} - \mathbf{X}_{ij}) \tag{10}$$

where $\mathbf{x}_{ij}$ and $\mathbf{X}_{ij}$ represent the interbead vector in the current and reference configurations, respectively.[29] The reference configurations are taken as the preshock structures, and the scalar slip $s_i = |\mathbf{s}_i|$ is used in our analysis. Although the slip vector approach was originally developed for crystalline materials,[29] it has proven to be a valuable tool for probing plastic deformation in amorphous materials.[27,30] Shock profiles of particle velocity u_p and slip magnitudes s along the z

dx.doi.org/10.1021/ma3001934 | Macromolecules 2012, 45, 3247–3255

direction are obtained via 1D binning procedure (averaging over beads residing within equal-sized "bins" along the shock direction[26,31]).

All MD simulations in this study are performed using the large-scale atomic/molecular massively parallel simulator (LAMMPS) package, developed by Sandia National Laboratories.[32]

3. RESULTS

Polymer Microstructure. Figure 2a,b shows representative configurations of the block copolymers H_2S_8 (diblock) and

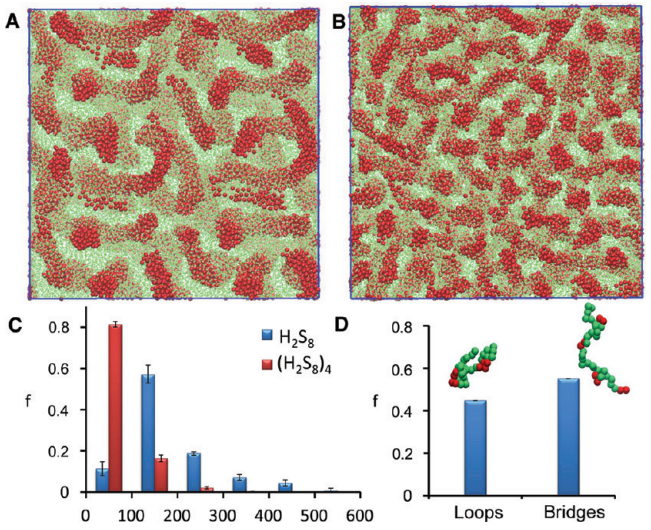

Figure 2. (a,b) Snapshot of the simulation box (of size 45.49σ) illustrating microphase separation of H_2S_8 and $(H_2S_8)_4$ into hard and soft domains. For visualization purposes, the H beads are represented by red spheres and the S beads by green points. (c) Size distribution of hard domains in H_2S_8 and $(H_2S_8)_4$ in terms of fraction of domains with sizes 0−100, 100−200 beads, and so on. (d) Fraction of soft segments in $(H_2S_8)_4$ that form loops and bridges.

$(H_2S_8)_4$ (multiblock) taken from our MD simulations following extensive equilibration. Both block copolymers undergo microphase separation into rod-shaped hard domains composed of H beads surrounded by a soft domain composed of S beads. However, the two block copolymers show distinct differences in their morphology. Whereas H_2S_8 displays thick, long, and strongly segregated hard domains, $(H_2S_8)_4$ displays thinner, shorter, and less strongly segregated hard domains. The diameters of the rod-like hard domains fall in the range $5-8\sigma$ (6−10 nm) for H_2S_8 and $4-7\sigma$ (5−8 nm) for $(H_2S_8)_4$. These sizes agree well with the reported diameters of 5−10 nm for poly(urethane urea) hard domains obtained via AFM tapping measurements.[33] To explore these differences further, we have computed the size distribution of the hard domains for both block copolymers (Figure 2c). H_2S_8 exhibits a broad size distribution of hard domains containing 76−540 H beads with ∼57% of the domains containing 100−200 beads. $(H_2S_8)_4$ exhibits a narrower size distribution of hard domains containing 25−280 H beads with ∼80% of the domains containing 0−100 beads. Because the number of hard segments is the same in both systems, H_2S_8 segregates into a smaller number of hard domains (∼85) compared with $(H_2S_8)_4$ (∼211). The fact that $(H_2S_8)_4$ yields smaller hard domains than H_2S_8 can be explained based on the connectivity restraint between the hard segments of a chain, which imposes a large entropic and energetic penalty for the hard segments from the same or different chains to participate in the formation of hard domains. Stronger entanglements effects in the case of the longer $(H_2S_8)_4$ chains further hinder the formation of large hard domains.

The hard segments of a single multiblock copolymer chain can be involved in more than one hard domain, allowing for hard domains to be connected to each other via intervening soft segments. To investigate the degree of connectivity between hard domains, we have computed the fraction of soft segments that "bridge" across distinct hard domains, as denoted by f_{bridge}, and the fraction that "loop" to allow two hard segments to participate in a common hard domain, as denoted by $f_{loop} \approx 1 - f_{bridge}$. Therefore, f_{bridge} quantifies the degree of connectivity between the hard domains while f_{loop} quantifies their independence. The results of such an analysis are shown in Figure 2d, indicating that the hard domains are well-connected to each other. In fact, more than half of the soft segments (f_{bridge} = 0.56) are involved in connections between hard domains.

Figure 3 presents the radial distribution functions $g(r)$ for the three pairwise interactions $H-H$, $S-S$, and $H-S$ in the H_2S_8

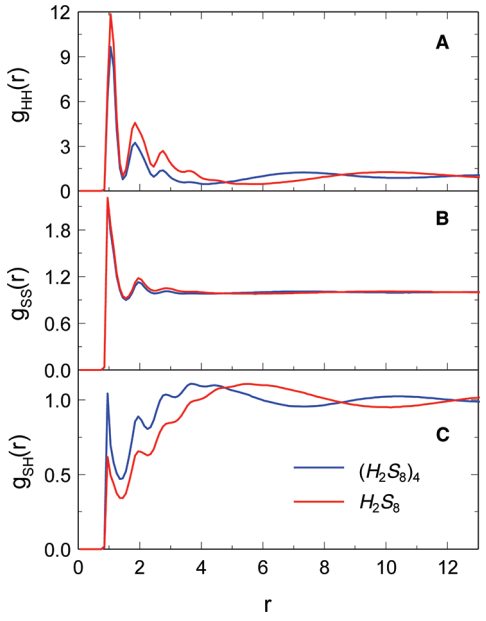

Figure 3. Radial distribution functions of (a) $H-H$, (b) $S-S$, and (c) $S-H$ beads compared for H_2S_8 (red lines) and $(H_2S_8)_4$ (blue lines).

and $(H_2S_8)_4$, where r is the separation distance between the polymer beads. The distributions reveal key structural differences between the hard and soft domains as well as differences between the domain morphology of the diblock and multiblock copolymers. First, the shallow, long-range peak in g_{HH} (Figure 3a), which corresponds to the average separation between hard domains, indicates that the interdomain distances are larger ($\sim 10\sigma$) in H_2S_8 compared with $(H_2S_8)_4$ ($\sim 7\sigma$). This result is expected given the smaller number of larger-sized hard domains in the diblock copolymer compared with the multiblock copolymer. Second, the considerably higher short-range peak in g_{HH} (Figure 3a) compared with g_{SS} (Figure 3b) reflects a near-crystalline solid structure of the hard domains compared with the more fluid-like structure of the soft domains, in agreement with the expected morphology of polyurea. Third, this g_{HH} peak is somewhat lower in $(H_2S_8)_4$ compared with

dx.doi.org/10.1021/ma3001934 | Macromolecules 2012, 45, 3247−3255

H_2S_8, indicating less compact and segregated hard domains in the former system. Fourth, the higher short-range peaks in the g_{SH} of $(H_2S_8)_4$ (Figure 3c) are reflective of the larger number of bonded $H-S$ segments.

Viscoelastic Properties. The Newtonian shear viscosity η of the diblock and multiblock copolymers and of the corresponding homopolymers has been obtained using eqs 4−6. As expected, $(H_2S_8)_4$ with $\eta = 2232 \pm 312$ is more viscous than H_2S_8 with $\eta = 498 \pm 122$ because of the longer chains and the network-like connectivity of the hard domains previously discussed. Also, as expected, the two copolymers exhibit a significantly higher viscosity than their corresponding homopolymers S_{40} and S_{10}, with $\eta = 33.7 \pm 3.2$ and 10.2 ± 1.3, respectively. The viscosities of the two homopolymers are in good agreement with previously computed values.[34]

The dynamic shear modulus $G(t)$ of the two block copolymers and of the two homopolymers are plotted in Figure 4. To reduce the large noise present in $G(t)$ at longer

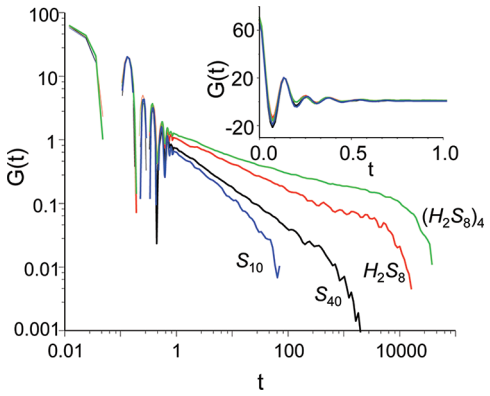

Figure 4. Dynamic shear modulus $G(t)$ for S_{10} (blue), S_{40} (black), H_2S_8 (red), and $(H_2S_8)_4$ (green) in log−log scale. The inset shows the short-time behavior of $G(t)$ in regular scale.

times, we report running averages from $0.9t$ to $1.1t$ for each time, t, as suggested by a previous study.[34] At short times $t = 0$ to 1.0, the primary mechanism for stress relaxation is the rearrangement of bond lengths and is independent of the microstructure. Therefore, the $G(t)$ values for the four polymeric systems are similar at short times (Figure 4 inset). At intermediate times, the reorientation of chain segments becomes more dominant for relaxing polymer conformations and the $G(t)$ values for the four systems begin to differ. Because we do not expect any significant entanglement effects in homopolymers of lengths 10 and 40 beads,[34] their $G(t)$ roughly follow the Rouse scaling $t^{-1/2}$. Significant "slowing down" and deviations from the Rouse scaling are observed in the case of the two block copolymers. We also observe a hint of a plateau in the $G(t)$ of the block copolymers, which is more apparent in $(H_2S_8)_4$ than H_2S_8. Such plateauing is indicative of a solid-like response stemming from the immobilization of hard segments within the hard domains. The network-like connectivity of hard domains also likely contributes to this effect in the case of multiblock copolymers. A similar looking but more prominent plateau was recently observed in the $G(t)$ of polymer nanocomposites[35,36] that was attributed to the lower mobility of polymer segments near particle surfaces. Therefore, the block copolymers' response are intermediate to that of homopolymer melts and polymer nanocomposites. At even longer times, all $G(t)$ drop precipitously in an exponential manner with a time constant given by the longest relaxation mode in the system.[34] The fact that we observe such a drop suggests that the MD simulations are sufficiently long to capture the mechanisms responsible for stress relaxation and that the plateauing effect might be real and not an artifact of the time-limitation of MD simulations.

The storage $G'(\omega)$ and loss $G''(\omega)$ moduli of the four polymers, as computed via eqs 8 and 9, are plotted in Figure 5.

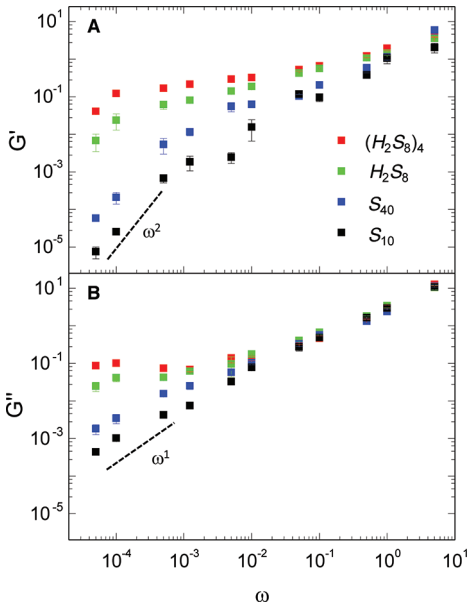

Figure 5. Storage G' and loss G'' moduli as a function of frequency ω for S_{10} (blue), S_{40} (black), H_2S_8 (red), and $(H_2S_8)_4$ (green). The dashed lines in the G' and G'' representing ω^2 and ω^1 scalings are included as guides.

The viscoelastic response at low frequencies is strongly indicative of the state of the material.[18] The homopolymers show liquid-like terminal behavior at low frequencies, that is, $G' \approx \omega^2$ and $G'' \approx \omega^1$. In contrast, the diblock and multiblock copolymer show departure from the above scalings in the same frequency range with $G' \approx \omega^\nu$ and $G'' \approx \omega^\mu$, where $\nu < 2$ and $\mu < 1$. This nonterminal behavior indicates that the two block copolymer systems behave as an intermediate to a Newtonian fluid ($G'' \approx \omega^1$) and a solid ($G'' \approx \omega^0$), as expected for block copolymers below their order−disorder temperature.[18,37] This loss of terminal liquid-like behavior in both $G'(\omega)$ and $G''(\omega)$ is more prominent in $(H_2S_8)_4$ than H_2S_8. Interestingly, $(H_2S_8)_4$ exhibits the largest storage and loss modulus across the entire frequency range, followed by H_2S_8, then S_{40} and S_{10}. The higher $G'(\omega)$ in $(H_2S_8)_4$ is expected given its higher elasticity arising from the more networked, hard domains, but the fact that the networked structure of $(H_2S_8)_4$ also yields a higher loss modulus is not so obvious. How exactly the connectivity between hard domains leads to higher dissipation is not clear but could arise from concerted motions of the interconnected hard domains. A similar result has been observed experimentally in block copolymers possessing hard A (diamide) and soft B (poly(tetramethylene oxide)) segments, where multiblock polymers $(AB)_4$ exhibit higher overall modulus than triblock ABA_7 and diblock copolymers AB_3.[38]

The general shapes of the computed $G'(\omega)$ and $G''(\omega)$ for the two block copolymers agree well with those measured experimentally for cubic and bicontinuous microphase-forming

dx.doi.org/10.1021/ma3001934 | Macromolecules 2012, 45, 3247−3255

block copolymers.[39,40] At low frequencies, $G'(\omega) < G''(\omega)$ and the material is more dissipative than elastic. At intermediate frequencies, a crossover occurs and the material becomes more elastic, that is, $G'(\omega) > G''(\omega)$. At the onset of this regime, the $G'(\omega)$ and $G''(\omega)$ exhibit a plateau and a dip, respectively, which are typically indicative of entanglement effects. Note that the block copolymers studied here are too short to exhibit true chain entanglements. Hence, the observed plateauing effect most likely arises from the immobilization of the H segments of the polymer chains within the hard domains. At higher frequencies, $G''(\omega)$ and $G'(\omega)$ both rise monotonically in a manner similar to homopolymers until $G'(\omega) < G''(\omega)$ again. This ω-dependent modulation in the "dissipativeness" of the two block copolymers may also be gleaned from calculations of $\tan \delta$ $[= G''(\omega)/G'(\omega)]$ provided in the Supporting Information, Figure S1.

In general, the sensitivity of $G'(\omega)$ and $G''(\omega)$ to the microstructure diminishes above a critical frequency ω_c roughly given by $0.1\tau^{-1}$, where τ is the single-chain terminal relaxation time estimated from the frequency at which $G'(\omega)$ and $G''(\omega)$ cross.[37] For our polymer systems, one can obtain $\omega_c \approx 0.01$ from Figure 5. Therefore, according to the above argument, the $G'(\omega)$ and $G''(\omega)$ curves are supposed to become similar for all systems for $\omega > \omega_c$. Whereas $G''(\omega)$ curves follow this rule, as noted by their rapid convergence for $\omega > \omega_c$, the $G'(\omega)$ curves converge much slower. In particular, the distinction between all four polymers remains until $\omega \approx 0.5$, even though the diblock and multiblock copolymer $G'(\omega)$ seems to have converged by $\omega \approx \omega_c$. Such lower sensitivity of $G''(\omega)$ compared with $G'(\omega)$ has also been observed in experiments and theoretical models.[37,41]

Shock Response. The two block copolymers and the S_{40} homopolymer were subjected to shock loading with a particle velocity u_p in the range 0.25 to 3.0. Figure 6a,b shows representative shocked-state configurations of $(H_2S_8)_4$ and H_2S_8 for $u_p = 2$, illustrating the differences in the polymer microstructure across the shock-unshocked interface. The corresponding u_p–z profiles for the two systems recorded at equivalent time intervals after shock initiation are shown in Figure 6c; here z specifies position along the shock direction and u_p is the measured particle velocity. The above profiles demonstrate the existence of well-supported shocks and also illustrate differences in the shock velocities developed within the two systems.

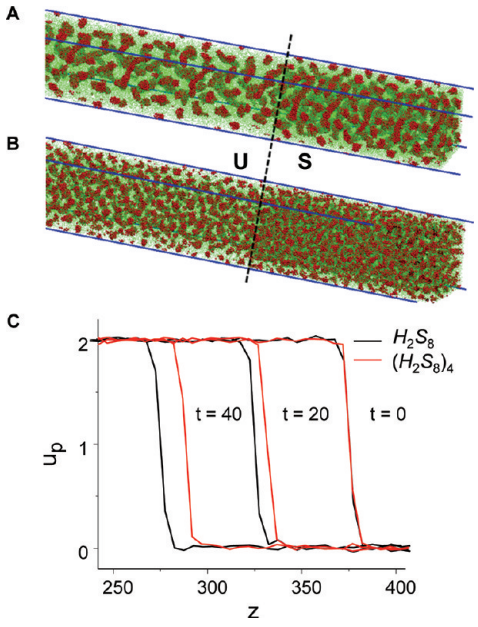

Figure 6. (a,b) Representative configurations of H_2S_8 (a) and $(H_2S_8)_4$ (b) captured from shock simulation illustrating the shock front (dotted line) separating the unshocked region (U) from the shocked (S) regions. The H beads are shown as red spheres and the S beads as green dots. (c) Particle velocity $u_p(x)$ profiles for H_2S_8 (black) and $(H_2S_8)_4$ (red).

In Figure 7, we have plotted the shock velocity u_s as a function of particle velocity u_p, commonly referred to as the u_s–u_p Hugoniot, for the three systems investigated here. The shock velocities have been computed from the rate of propagation of the shock front with time. A linear dependence between u_s and u_p across the investigated range of particle velocities is observed. A similar linear relationship has also seen in the experimental shock response of polyurea-1000.[42] More importantly, we find $(H_2S_8)_4$ consistently exhibits a lower u_s than H_2S_8, and the difference between the two becomes more pronounced at $u_p > 1.0$. This difference in shock speeds can also be gleaned from the shock profiles shown in Figure 6c. Overall, $(H_2S_8)_4$ shows shock velocities comparable to the homopolymer S_{40}.

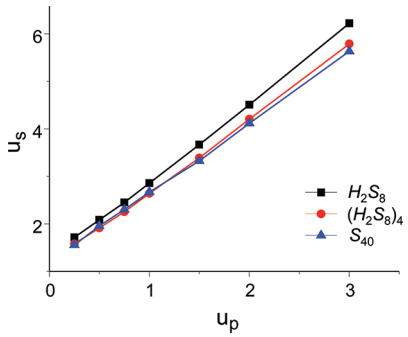

Figure 7. Computed u_s–u_p Hugoniot for the H_2S_8 (black squares), $(H_2S_8)_4$ (red circles), and S_{40} (blue triangles).

To investigate the molecular origin of the lower shock velocity in the multiblock copolymer as compared to the diblock copolymer, we have computed the magnitudes s of the slip vector for each polymer bead in the two block copolymers according to eq 10. The difference between the slip magnitude s of shocked and unshocked material roughly quantifies the amount of plastic deformations associated with shock propagation. Figure 8a,c shows representative snapshots of the diblock and multiblock copolymer configurations, shock-loaded at $u_p = 2$, in which each polymer bead has been color-coded according to the magnitude of the slip vector s. To match the computed s with the bead type (H or S), we have also included another representation in which polymer beads are now colored according to their type (Figure 8b,d). We have also computed the overall slip magnitudes s and the individual slip values of the H and S segments across the shock front as a function of position z along the shock direction (Figure 9a,b).

Figures 8 and 9 show that for both block copolymers the unshocked regions exhibit a finite slip as a result of thermal fluctuations and that the slip increases nearly two-fold in the shocked regions. More importantly, the slip profiles $s(z)$ in Figure 9a reveal that whereas H_2S_8 exhibits a larger slip ($s \approx 3.2$) than $(H_2S_8)_4$ ($s \approx 2.8$) in the unshocked regions, both

dx.doi.org/10.1021/ma3001934 | Macromolecules 2012, 45, 3247–3255

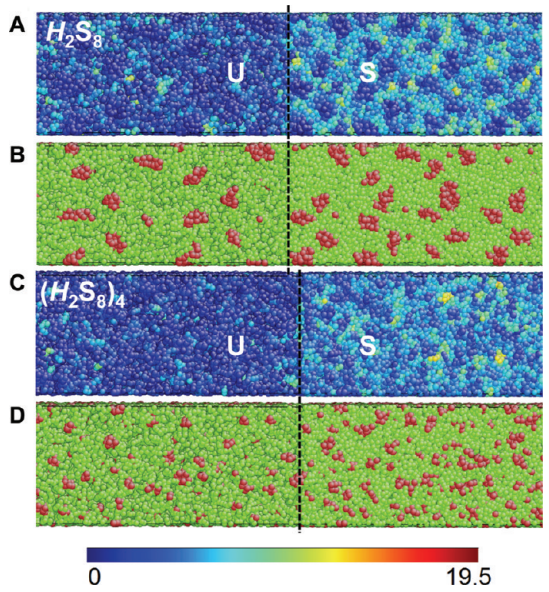

Figure 8. Slip magnitude s of H_2S_8 (a) $(H_2S_8)_4$ (c) beads according to the included color scheme. The corresponding color representations according to bead type are shown in (b) and (d), respectively. The H and S beads are shown as red spheres and green dots, respectively. The labels U and S indicate unshocked and shocked regions, which are separated the dotten line. The visualization is created via AtomEye.[49]

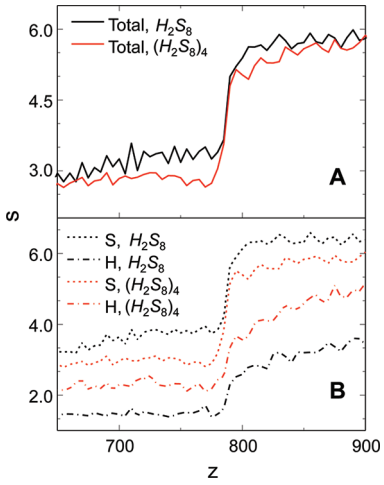

Figure 9. (a) Total slip s profiles along the z direction (solid lines) and (b) contributions from H (dotted-dashed lines) and S (dotted lines) beads for H_2S_8 (black lines) and $(H_2S_8)_4$ (red lines) at $u_p = 2$.

copolymers exhibit higher and more comparable slips in the shocked region with $s \approx 5.9$ for H_2S_8 and $s \approx 5.7$ for $(H_2S_8)_4$. The difference in s between the shocked (S) and unshocked (U) regions, $\Delta s \equiv s_S - s_U$, suggests that $(H_2S_8)_4$ undergoes an overall larger deformation ($\Delta s = 2.9$) upon shock than H_2S_8 ($\Delta s = 2.7$). The individual slip profiles $s(z)$ in Figure 9b reveal that the H beads undergo larger jumps in the slip Δs across the shock front in $(H_2S_8)_4$ ($\Delta s \approx 2.7$) as compared with H_2S_8 ($\Delta s \approx 2.0$). The S beads exhibit similar jumps $\Delta s \approx 2.9$ in both $(H_2S_8)_4$ and H_2S_8. The lower jump Δs of the H beads for H_2S_8 reflects a higher conservation of hard domains in H_2S_8 under shock loading as compared with $(H_2S_8)_4$. This difference between the two block copolymers can also be observed from the greater conservation of the dark blue regions (corresponding to the hard domains) across the shock front in the slip representation of H_2S_8 (Figure 8a) compared with that of $(H_2S_8)_4$ (Figure 8c). Therefore, the hard domains in the diblock copolymer essentially behave as rigid bodies with high shock impedance resulting in increased u_s, similar to recent studies on carbon nanotube composites.[27,43] Multiblock copolymers show an overall more homogeneous s distribution for both hard and soft segments in the shocked state, indicating that the H beads are possibly more open to deformation upon shock loading. In other words, whereas the soft segments carry most of the plastic deformation in H_2S_8, both the soft and hard segments are equally involved in carrying plastic deformations in $(H_2S_8)_4$. The above analyses thus suggest that the stronger dissipation and lower shock speeds observed in the multiblock copolymer in relation to diblock copolymers might arise from the larger deformability of the hard domains of the multiblock copolymer.

Our slip analyses reveals several additional insights. First, the S segments contribute the most slip in both block copolymers (Figure 9b). These strongly slipping S beads can be seen as the light blue colored beads in Figure 8a,c. The higher s of the S beads is understandable given their higher mobility compared with the H beads, which are trapped within hard domains. A similar reasoning explains why the S beads of H_2S_8 chains exhibit higher s and are more mobile than those of $(H_2S_8)_4$ chains; that is, only one end of the S segment is trapped in the hard domains of diblock copolymers, whereas both of its ends are trapped in multiblock copolymers. Second, as expected, the H segments (red beads) in both copolymers are more densely packed in the shocked state compared with the unshocked region (Figure 8). Because of the higher deformability of the multiblock copolymer compared with the diblock copolymer, one expects the multiblock copolymer to exhibit a higher relative increase in density ρ_S/ρ_U across the shock front. Given the well-known relationship between the shock and particle speeds $u_s = u_p/(1 - \rho_S/\rho_U)$ arising from mass balance,[44] one can conclude that the more deformable multiblock copolymer should naturally exhibit lower shock speeds. Third, the shock front in Figure 9b shows critical differences between the H and S beads. The s values of the S beads in both copolymers exhibit a sharp jump at the shock front and also approach a steady value quickly. The s values for the H beads, in contrast, display a more gradual transition to the shocked state, yielding a broader shock front. The more gradual shock front in the H beads might result from their higher viscosity (compared with S beads) because there exists an inverse relationship between effective viscosity and steepness of the shock front.[43,45]

4. DISCUSSION

We have used a computational approach to provide insight into how the multiblock chain architecture of polyurea, composed of repeating units of "hard" and "soft" segments, might endow it with structural and dynamical properties suitable for energy dissipation. Specifically, we have carried out MD simulations to compute and compare the microstructure, viscoelastic properties, and shock response of a polyurea-like multiblock copolymer, its diblock copolymer counterpart, and two homopolymers of similar molecular weights composed of only soft segments.

Our equilibrium simulations demonstrate that the multiblock copolymer microphase-separates into rod-shaped hard domains dispersed within a soft matrix. Because of the strong restraints on chain conformations in multiblock copolymer limiting its microphase separation, the hard domains are smaller and more

dx.doi.org/10.1021/ma3001934 | Macromolecules 2012, 45, 3247−3255

uniformly sized compared with those of the diblock copolymer. Examination of chain conformations reveals that about half of the soft segments in the multiblock copolymer are involved in bridging interactions across hard domains, whereas the remaining half yield loops connected to the same hard domain. The radial distribution functions for the interactions between the hard segments reveal a more strongly segregated, crystalline structure of the hard domains in the diblock copolymer compared with the multiblock copolymer. A comparison of the viscoelastic properties of the polymers reveals that the multiblock copolymer possesses a higher storage and loss modulus relative to the diblock copolymer and the homopolymers. We have also investigated the dynamic response of the polymers under shock loadings. Our shock simulations reveal that the shock wave propagates slower in the multiblock copolymer relative to its diblock counterpart. Deformation analysis based on slip vector calculation reveals that the hard segments undergo larger deformations across the shock front in multiblock copolymer in comparison with those in the diblock copolymer.

The observed differences between the properties of multiblock and diblock copolymers provide important insight into how the multiblock chain architecture of polyurea might endow it with superior dissipative properties. First, the networked structure observed in multiblock copolymers, where the hard domains are linked to each other via soft segments, allows hard domain motions to be coupled. Such coupling might enhance energy dissipation in polyurea through concerted, resonant motions of the hard domains,[7] which help trap the energy of a pressure/shock wave. The trapped energy can then be dissipated through the soft segments. The superior dissipative properties of the multiblock copolymer are evident from its larger loss modulus and lower shock velocities relative to those of the diblock copolymer. Second, our microstructure analyses suggest that the multiblock architecture of polyurea likely prevents its microphase segregation into large, strongly segregated hard domains. The resulting hard domains that are smaller and more weakly segregated are therefore easier to deform or dissociate when a shock or pressure wave passes through the material. Indeed, our shock simulations capture the stronger deformation of the multiblock copolymer hard domains compared with those of the diblock copolymer. Such deformations in the hard domains, along with their possible dissociation, have the potential to absorb large amounts of energy, thereby enhancing dissipation.

In conclusion, the current study lays the groundwork for future computational studies on the structure−function relationship of polyurea with the ultimate goal of enhancing its dissipative properties by tuning its molecular architecture. One possible direction is to examine how other parameters linked to block copolymers,[37] such as the chain length, the ratio of the hard and soft segments, and the degree of segregation (Φ) affect the viscoelastic properties and shock response of multiblock copolymers. Another direction is the development of higher resolution, coarse-grained models of polyurea through approaches like force-matching[46] and iterative Boltzmann inversion[47] that treat more accurately the specific and directional interactions in polyurea. A third future direction is examining how the energy from shock waves could be scattered or redirected through control over the alignment of anisotropic hard domains, which will aid ongoing experimental work in this area.[48]

■ ASSOCIATED CONTENT

Ⓢ Supporting Information

Plot of tan δ versus ω for the four polymeric systems investigated here. This material is available free of charge via the Internet at http://pubs.acs.org.

■ AUTHOR INFORMATION

Corresponding Author

*E-mail: garya@ucsd.edu. Phone: 858-822-5542. Fax: 858-534-9553.

Notes

The authors declare no competing financial interest.

■ ACKNOWLEDGMENTS

We thank Dr. Roshdy Barsoum, Prof. Sia Nemat-Nasser, Dr. Alireza Amirkhizi, Dr. Jay Oswald, Dr. Davide Hill, and Darren Yang for useful discussions. This work has been partially supported through ONR under grant no. N00014-09-1-1126 to the University of California, San Diego. Computations were performed at the Northwestern University Supercomputing Facility.

■ REFERENCES

(1) Das, S.; Cox, D. F.; Wilkes, G. L.; Klinedinst, D. B.; Yilgor, I.; Yilgor, E.; Beyer, F. L. *J. Macromol. Sci., Part B* **2007**, *46*, 853.
(2) Chattopadhyay, D. K.; Raju, K. V. S. N. *Prog. Polym. Sci.* **2007**, *32*, 352.
(3) http://www.polyurea.com/ (accessed Jan 15, 2012).
(4) Bogoslovov, R. B.; Roland, C. M.; Gamache, R. M. *Appl. Phys. Lett.* **2007**, *90*, 221910.
(5) Xue, L.; Mock, W. Jr.; Belytschko, T. *Mech. Mater.* **2010**, *42*, 981.
(6) Grujicic, M.; Pandurangan, B.; He, T.; Cheeseman, B. A.; Yen, C. F.; Randow, C. L. *Mater. Sci. Eng., A* **2010**, *527*, 7741.
(7) Qiao, J.; Amirkhizi, A. V.; Schaaf, K.; Nemat-Nasser, S.; Wu, G. *Mech. Mater.* **2011**, *43*, 598.
(8) Grujicic, M.; Pandurangan, B.; Bell, W. C.; Cheeseman, B. A.; Yen, C. F.; Randow, C. L. *Mater. Sci. Eng., A* **2011**, *528*, 3799.
(9) Kremer, K.; Grest, G. *J. Chem. Phys.* **1990**, *92*, 5057.
(10) Tekalur, S. A.; Shukla, A.; Shivakumar, K. *Compos. Struct.* **2008**, *84*, 271.
(11) Gardner, N.; Wang, E.; Kumar, P.; Shukla, A. *Exp. Mech.* **2012**, *52*, 119.
(12) Amirkhizi, A. V.; Isaacs, J.; McGee, J.; Nemat-Nasser, S. *Philos. Mag.* **2006**, *86*, 5847.
(13) Weeks, J.; Chandler, D.; Andersen, H. *J. Chem. Phys.* **1971**, *54*, 5237.
(14) Soddemann, T.; Dunweg, B.; Kremer, K. *Eur. Phys. J. E* **2001**, *6*, 409.
(15) Guo, H.; Kremer, K. *J. Chem. Phys.* **2003**, *118*, 7714.
(16) Arya, G.; Rottler, J.; Panagiotopoulos, A.; Srolovitz, D.; Chaikin, P. *Langmuir* **2005**, *21*, 11518.
(17) Arya, G.; Panagiotopoulos, A. *Phys. Rev. Lett.* **2005**, *95*, 188301.
(18) Larson, R. G. *The Structure and Rheology of Complex Fluids*; Oxford University Press: New York, 1999.
(19) Cahoon, J. R. *Can. J. Phys.* **2004**, *82*, 291.
(20) Grujicic, M.; Pandurangan, B.; King, A. E.; Runt, J.; Tarter, J.; Dillon, G. *J. Mater. Sci.* **2011**, *46*, 1767.
(21) Nose, S. *Prog. Theor. Phys. Suppl.* **1991**, *103*, 1.
(22) Auhl, R.; Everaers, R.; Grest, G. S.; Kremer, K.; Plimpton, S. J. *J. Chem. Phys.* **2003**, *119*, 12718.
(23) Sukumaran, S. K.; Likhtman, A. E. *Macromolecules* **2009**, *42*, 4300.
(24) Likhtman, A. E.; Sukumaran, S. K.; Ramirez, J. *Macromolecules* **2007**, *40*, 6748.
(25) Holian, B. L. *Shock Waves* **1995**, *5*, 149.

(26) Luo, S. N.; Han, L.-B.; Xie, Y.; An, Q.; Zheng, L. Q.; Xia, K. *J. Appl. Phys.* **2008**, *103*, 093530.
(27) Arman, B.; An, Q.; Luo, S. N.; Desai, T. G.; Tonks, D. L.; Cagin, T.; Goddard, W. A. III. *J. Appl. Phys.* **2006**, *109*, 13503.
(28) Brandl, C. Ph.D. Thesis No. 4591, Ecole Polytechnique Fédérale de Lausanne, 2009.
(29) Zimmerman, J. A.; Kelchner, C. L.; Klein, P. A.; Hamilton, J. C.; Foiles, S. M. *Phys. Rev. Lett.* **2001**, *87*, 165507.
(30) Lee, W.-J.; Ju, S.-P.; Cheng, C.-H. *Langmuir* **2008**, *24*, 13440.
(31) Arman, B.; Luo, S.-N.; Germann, T. C.; Cagin, T. *Phys. Rev. B* **2010**, *81*, 144201.
(32) http://lammps.sandia.gov (accessed Jan 15, 2012).
(33) Garrett, J. T.; Siedlecki, C. A.; Runt, J. *Macromolecules* **2001**, *34*, 7066.
(34) Sen, S.; Kumar, S.; Keblinski, P. *Macromolecules* **2005**, *38*, 650.
(35) Thomin, J. D.; Keblinski, P.; Kumar, S. K. *Macromolecules* **2008**, *41*, 5988.
(36) Smith, G.; Bedrov, D.; Li, L.; Byutner, O. *J. Chem. Phys.* **2002**, *117*, 9478.
(37) Fredrickson, G.; Bates, F. *Annu. Rev. Mater. Sci.* **1996**, *26*, 501.
(38) Arun, A.; Dullaert, K.; Gaymans, R. J. *Polym. Eng. Sci.* **2010**, *50*, 756.
(39) Zhao, J.; Majumdar, B.; Schulz, M. F.; Bates, F. S.; Almdal, K.; Mortensen, K.; Hajduk, D. A.; Gruner, S. M. *Macromolecules* **1996**, *29*, 1204.
(40) Sebastian, J. M.; Graessley, W. W.; Register, R. A. *J. Rheol.* **2002**, *46*, 863.
(41) Zhang, Z.; Zhang, H.; Yang, Y.; Vinckier, I.; Laun, H. *Macromolecules* **2001**, *34*, 1416.
(42) Mock, W.; Bartyczak, S.; Lee, G.; Fedderly, J.; Jordan, K. Dynamic Properties of Polyurea 1000. In *Shock Compression of Condensed Matter*; American Institute for Physics: Melville, NY, 2009; Vol. *1195*.
(43) Makeev, M. A.; Sundaresh, S.; Srivastava, D. *J. Appl. Phys.* **2009**, *106*, 014311.
(44) Holian, B. L.; Hoover, W. G.; Moran, B.; Straub, G. K. *Phys. Rev. A* **1980**, *22*, 2798.
(45) Hoover, W. G. *Phys. Rev. Lett.* **1979**, *42*, 1531.
(46) Ercolessi, F.; Adams, J. B. *Europhys. Lett.* **1994**, *26*, 583.
(47) Reith, D.; Putz, M.; Muller-Plathe, F. *J. Comput. Chem.* **2003**, *24*, 1624.
(48) Amirkhizi, A. V.; Tehranian, A.; Nemat-Nasser, S. *Wave Motion* **2010**, *47*, 519.
(49) Li, J. *Modell. Simul. Mater. Sci. Eng.* **2003**, *11*, 173.